



# Combustion synthesis and characterization of Mg-based Fe-doped biphasic calcium phosphate ceramics

Omer Kaygili<sup>1</sup>

Received: 2 April 2019 / Accepted: 21 May 2019 / Published online: 24 May 2019  
© Springer-Verlag GmbH Germany, part of Springer Nature 2019

## Abstract

Mg-based (0.35 at.%) biphasic calcium phosphates (BCPs) doped with Fe at various amounts (e.g., 0.35, 0.70 and 1.05 at.%) were prepared by the combustion method. The X-ray diffraction (XRD) analysis confirmed the biphasic structure, composed of hydroxyapatite (HAp) and beta-tricalcium phosphate ( $\beta$ -TCP) for each sample. While  $\beta$ -TCP content increases, HAp content decreases with increasing Fe levels. The crystallinity decreased with the addition of Fe. The unit cell parameters and crystallite size were affected by Fe content. The existence of both phosphate and hydroxyl groups in the samples was verified by the Fourier transform infrared (FTIR). A mass gain was observed for each BCP. The formation of the rod-shaped particles was observed.

## 1 Introduction

The members of calcium phosphate family are special bio-ceramic materials used in the medical applications [1]. There are 12 members of this family according to Dorozhkin's report [2]. Among these kinds, hydroxyapatite (HAp) and beta-tricalcium phosphate ( $\beta$ -TCP) are the most popular ones, and their chemical formulas are  $\text{Ca}_{10}(\text{PO}_4)_6(\text{OH})_2$  and  $\text{Ca}_3(\text{PO}_4)_2$ , respectively [3]. The combination of both phases is known as the biphasic calcium phosphate (BCP) structure [4]. BCPs have been widely used in bone reconstruction applications [5]. The osteoconductivity and osteoinductivity of the BCP were reported by Garai and Sinha [6]. The genotoxicity of the BCP was studied by Wahab et al. [7], and they reported that it showed a non-genotoxic effect. Mg-doped BCP is more useful than that of the un-doped one for biological applications [8]. The effects of both Fe-doping in various levels and applied sintering temperatures in the range of 500–1100 °C on the crystal structure and magnetic properties of the BCP were determined by Gomes et al. [9]. In the previous work, Fe-doped BCPs were synthesized via a wet chemical method and the as-obtained experimental results were reported in detail [10].

After making a detailed literature survey, there have been found a few reports mentioned above on Mg- and Fe-doped BCPs, whereas no study was found on the Mg/Fe co-doped BCPs in the literature. Therefore, in the present study, Mg-based BCPs with various Fe contents were synthesized using the combustion method and characterized in more detail via the XRD, FTIR, DTA, TGA and SEM. To the best of my knowledge, this is the first study on Mg-based BCPs in the literature.

## 2 Materials and methods

### 2.1 Synthesis

The chemicals of diammonium hydrogen phosphate (DAP,  $(\text{NH}_4)_2\text{HPO}_4$ ), calcium nitrate tetrahydrate (CN,  $\text{Ca}(\text{NO}_3)_2 \cdot 4\text{H}_2\text{O}$ ), magnesium nitrate hexahydrate (MN,  $\text{Mg}(\text{NO}_3)_2 \cdot 6\text{H}_2\text{O}$ ) and iron (III) nitrate nonahydrate (FN,  $\text{Fe}(\text{NO}_3)_3 \cdot 9\text{H}_2\text{O}$ ) purchased from the Sigma-Aldrich were used as the precursors of P, Ca, Mg and Fe, respectively. These chemicals were used as received without further purification, and the distilled water (DW) was used as the solvent. While Mg content was kept at a constant value of 0.35 at.%, Fe content was adjusted to 0.35, 0.70 and 1.05 at.%. Nominal amounts of the CN, MN and FN were dissolved in the DW in a beaker. (The total amount of this mixture is 100 ml.) An appropriate amount of 100 ml of the DAP was also dissolved in the DW in a different beaker and then

✉ Omer Kaygili  
okaygili@firat.edu.tr

<sup>1</sup> Department of Physics, Faculty of Science, Firat University,  
23119 Elazig, Turkey

added drop by drop to the CN, MN and FN mixture. A 15 ml of 0.5 M of urea ( $\text{CH}_4\text{N}_2\text{O}$ , Sigma-Aldrich) solution prepared in the DW was added to each sample as the fuel. The final mixture was continuously stirred in a magnetic stirrer at 85 °C for 1.5 h and then put into a furnace at 500 °C for 40 min. After putting into the furnace, the ignition was observed with dense smoke, which was continued during about 2 min. The as-dried sample was calcined at 850 °C for 3 h.

## 2.2 Characterization

To make a detailed crystal structure analysis, XRD data were recorded by a Rigaku RadB-DMAX II diffractometer using  $\text{CuK}\alpha$  radiation having the wavelength of  $\lambda = 0.154056$  nm in the  $2\theta$  range from 20 to 55°. A Perkin Elmer Spectrum One FTIR spectrometer was used to determine the functional groups found in the samples, and these measurements were carried out in the mid-infrared region (from 400 to 4000  $\text{cm}^{-1}$ ) using KBr pellets.

The morphological investigation of the samples was done using a LEO EVO 40xVP SEM operated at an accelerating voltage of 20 kV equipped with a Röntech xflash EDX spectrometer.

The investigation of the thermal behaviors of the as-synthesized samples in the temperature interval of 25–1000 °C at a heating rate of 10 °C  $\text{min}^{-1}$  was carried out using the Shimadzu DTA 50 and Shimadzu TGA 50.

## 3 Results and discussion

### 3.1 XRD results

The XRD patterns of the as-obtained BCPs in the  $2\theta$  range of 20–55° are shown in Fig. 1 together with the phase identifications and Miller indices ( $hkl$ ) for each diffraction plane. The determination of phase structure and quantitative analysis were performed using the XPowder software [11]. Each sample is composed of both hydroxyapatite (HAp with the hexagonal crystal structure, JCPDS PDF No: 09-0432) and beta-tricalcium phosphate ( $\beta$ -TCP with the rhombohedral crystal structure, JCPDS PDF No: 09-0169) phases, verifying the biphasic calcium phosphate structure. For all the samples, the major phase is  $\beta$ -TCP and the minor one is HAp. The amount of  $\beta$ -TCP phase increases gradually and that of HAp decreases dramatically with increasing Fe content (Table 1).

The crystallinity percent ( $X_C\%$ ) for each sample was calculated from the ratio of the total area under crystalline peaks to the total area under all observed peaks on the as-obtained XRD pattern [12]. The crystallinity percent decreases with the increase in the amount of Fe (Table 1). As reported, the crystallinity degree decreases with increasing amount of the  $\beta$ -TCP phase [13]. The gradual decrease in the  $X_C\%$  value can be associated with increasing Fe content, and this is in harmony with the results

**Fig. 1** XRD patterns of Mg-based BCPs doped with Fe

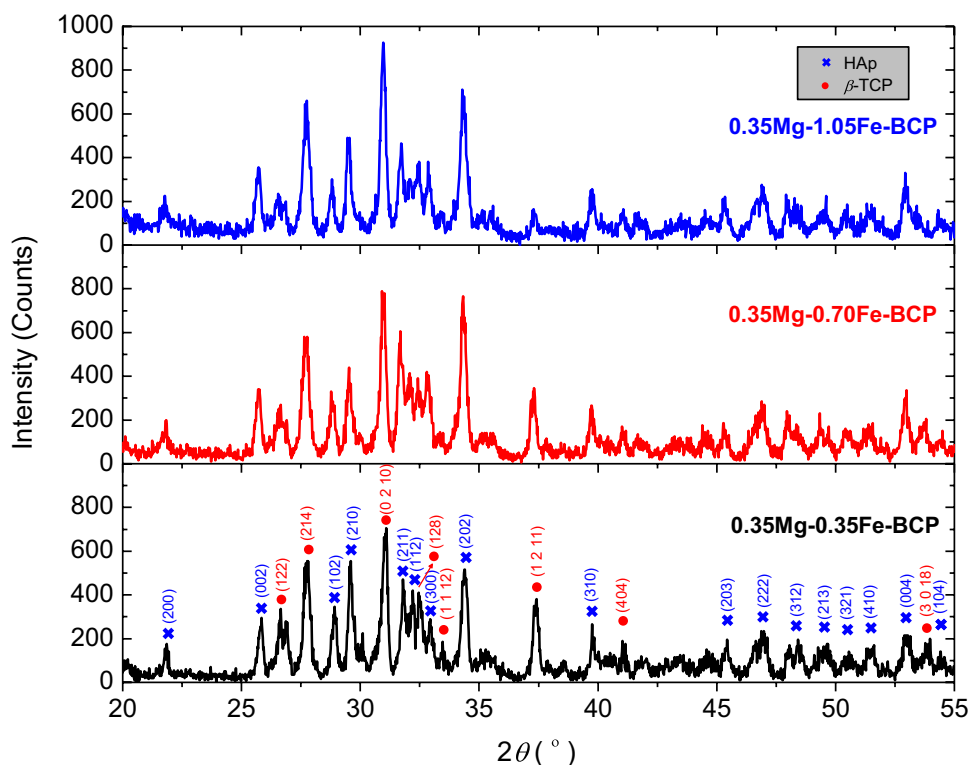


**Table 1** XRD related parameters of the as-synthesized BCPs

Sample	Phase composition (%)		$X_C\%$	HAp				$\beta$ -TCP			
	HAp	$\beta$ -TCP		$L_{002}$ (nm)	$a$ (nm)	$c$ (nm)	$V$ (nm <sup>3</sup> )	$L_{0210}$ (nm)	$a$ (nm)	$c$ (nm)	$V$ (nm <sup>3</sup> )
0.35 Mg–0.35Fe-BCP	40.0	60.0	86.5	29.96	0.9536	0.6890	0.5426	29.55	1.0435	3.7293	3.5167
0.35 Mg–0.70Fe-BCP	38.6	61.4	86.3	25.79	0.9451	0.6922	0.5354	30.42	1.0447	3.7409	3.5357
0.35 Mg–1.05Fe-BCP	33.4	66.6	84.7	25.38	0.9434	0.6812	0.5250	29.65	1.0459	3.7488	3.5513

found in the previous study [10]. The calculation of the crystallite size ( $L$ ) for each sample was done using the following Scherrer equation using the crystal planes of (0 0 2) and (0 2 10) for HAp and  $\beta$ -TCP phases, respectively [14]:

$$L = \frac{0.9\lambda}{\beta \cos \theta} \quad (1)$$

where  $\beta$  is the full width at half maximum and  $\theta$  is Bragg angle. For both phases, the crystallite size value is affected by Fe content. This value decreases gradually with the increasing amount of Fe for HAp phase.

The lattice parameters ( $a$  and  $c$ ) and unit cell volume ( $V$ ) values for HAp and  $\beta$ -TCP phases were estimated from Eqs. (2) and (3), respectively, using the hexagonal setting [14]:

$$\frac{1}{d^2} = \frac{4}{3} \left( \frac{h^2 + hk + k^2}{a^2} \right) + \frac{l^2}{c^2} \quad (2)$$

$$V = 0.866a^2c \quad (3)$$

where  $d$  is the distance for two adjacent planes. The  $a$ ,  $c$  and  $V$  values are affected by increasing Fe content. For the HAp phase, both  $a$  and  $V$  decrease gradually, whereas there is no gradual change in the  $c$  parameter. For  $\beta$ -TCP phase, these three parameters increase gradually. The ionic radii of both Mg<sup>2+</sup> (0.0650 nm) and Fe<sup>3+</sup> (0.0645 nm) ions are smaller than those of Ca<sup>2+</sup> (0.0990 nm) ion [15, 16]. According to this knowledge, the as-expected result is a gradual decrease in these three parameters for both phases. This may be explained as follows: For one of these dopants, the decrease in the abovementioned parameters can be expected, but in this study, two dopants were used together. Although their ionic radii are so close to each other, there is an imbalance between Mg<sup>2+</sup> and Fe<sup>3+</sup> ions, as well as Ca<sup>2+</sup> ions. It is assumed that every two Mg<sup>2+</sup> and two Fe<sup>3+</sup> should substitute with five Ca<sup>2+</sup> ions to ensure balance in the lattice. Mg was kept at a constant ratio for all the samples in this study. For increasing amounts of Fe, to provide the ionic balance, it can be assumed that every two Fe<sup>3+</sup> ions substitute with three Ca<sup>2+</sup> ions. The as-mentioned situations can cause more complex effects on the lattice structure different from the desired ones.

### 3.2 FTIR results

The assignments of the as-observed bands on the FTIR spectra of all the BCPs shown in Fig. 2 are given as follows. The band at 3676 cm<sup>-1</sup> is related to the hydroxyl group [17]. The phosphate group-related bands were detected at 1210, 1026, 972, 943, 601, 541, 495 and 455 cm<sup>-1</sup> [18–21]. The band observed at 1406 cm<sup>-1</sup> is associated with the carbonate group [22]. The carbonate group found in a BCP can be seen as an advantage for using it in the bone-healing applications since natural bone contains a small amount of carbonate [23, 24]. The bands of 2988 and 2901 cm<sup>-1</sup> are related to the methylene (CH<sub>2</sub>) group [25], probably originated from the synthesis precursor of urea. The as-obtained FTIR results confirmed the existence of the functional groups of both hydroxyl and phosphate of the BCP structure.

### 3.3 Morphology and elemental analysis

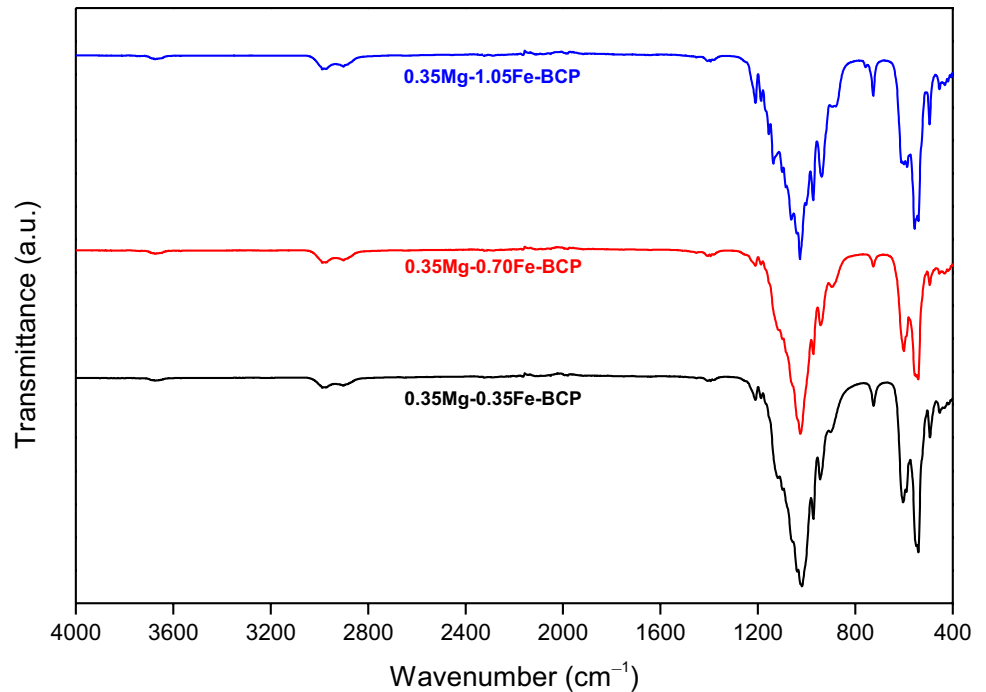
Figure 3 shows the SEM micrographs together with the EDX analysis results of the as-prepared BCPs. All the as-prepared BCPs are composed of the stacked rod-shaped particles. The EDX results confirm that all the samples include the elements of Ca, O, P, Mg and Fe, as expected, without any impurity. The introduction of both dopants into the BCP structure was confirmed for each sample. The as-detected Fe content increases with addition of Fe-dopant. Mg content was found to be in the range of 0.30–0.36%.

### 3.4 DTA and TGA results

The DTA curves of the as-synthesized BCPs in the range of 25–1000 °C are shown in Fig. 4. For all the samples, only one endothermic peak was observed. This peak was observed at 391, 395 and 398 °C for 0.35Mg–0.35Fe-BCP, 0.35Mg–0.70Fe-BCP and 0.35Mg–1.05Fe-BCP, respectively. The position of this peak began to shift to the right with increasing Fe content. This peak may be associated with the removal of crystalline water in the samples [26].

The TGA curves, taken in the as-mentioned temperature interval, point out that there is a mass gain for each sample. This increase is gradual for 0.35Mg–0.35Fe-BCP sample, whereas a negligible decrease in the mass percent (0.53 and

**Fig. 2** Plots of the FTIR spectra for all the samples

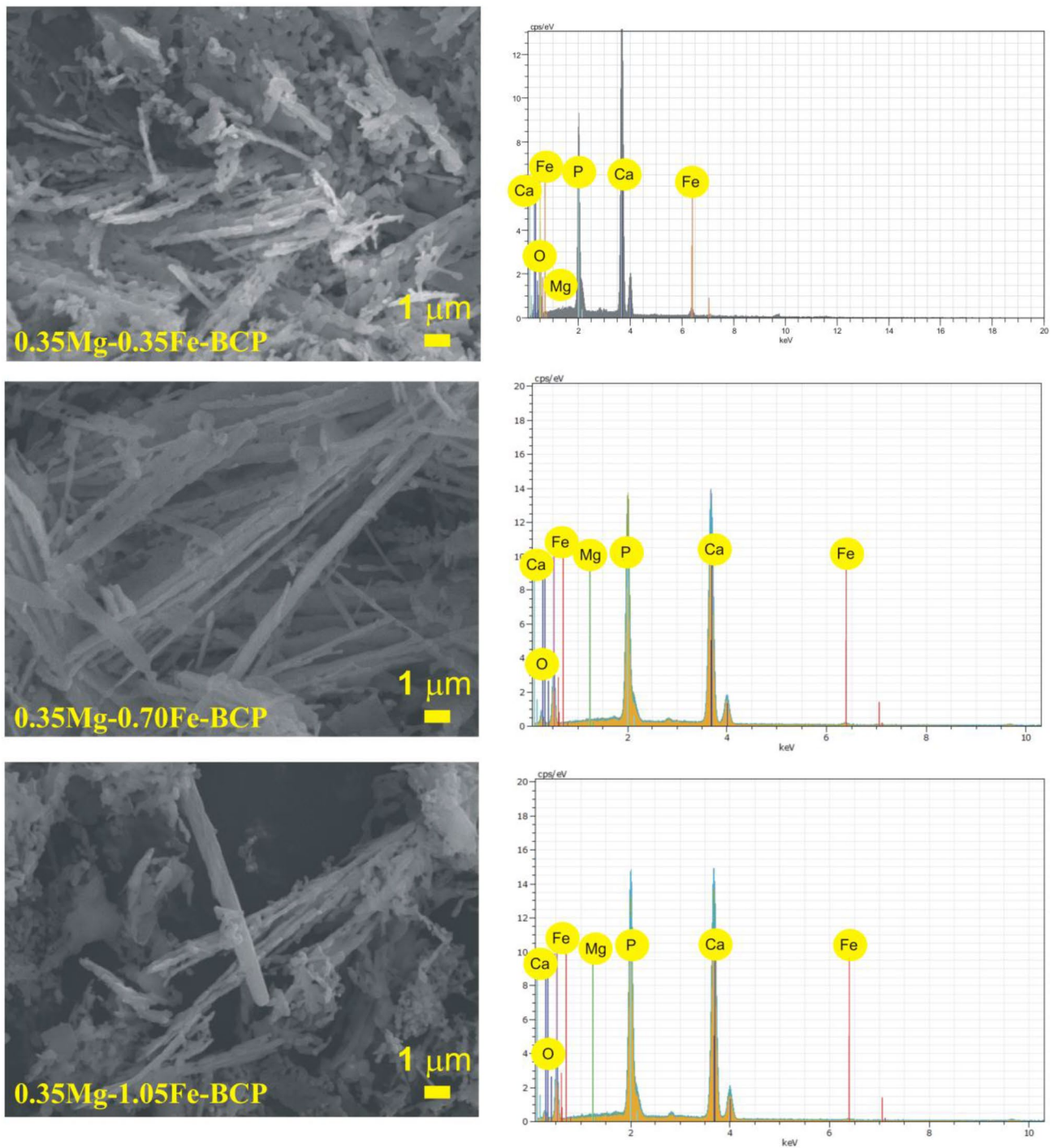


0.19%, respectively) was detected for both 0.35Mg–0.70Fe-BCP and 0.35Mg–1.05Fe-BCP samples at about in the range of 400–650 °C. At higher temperatures than this interval, a gradual mass gain starts for both samples. The overall mass gain at 1000 °C was found to be 1.93, 0.71 and 1.31% for 0.35Mg–0.35Fe-BCP, 0.35Mg–0.70Fe-BCP and 0.35Mg–1.05Fe-BCP, respectively. The TGA results are in a very good agreement with the literature [10, 27] (Fig. 5).

## 4 Conclusions

In this study, three Mg-based BCP samples doped with Fe at various amounts were produced by using the combustion method. After characterizing these samples using the XRD, FTIR, DTA, TGA and SEM, the following conclusions was reached: The XRD results support that all the samples have the biphasic structure, which is composed of both HAp and  $\beta$ -TCP phases. With the increase in Fe level, while the

crystallinity and amount of HAp phase decrease, the amount of  $\beta$ -TCP phase increases. All the crystal structure-related parameters investigated in this study are affected significantly by Fe content. The FTIR spectra confirm the formation of both hydroxyl and phosphate groups, which are the characteristic of the BCP structure. Once the thermal behaviors of the samples in the range from 25 to 1000 °C were investigated, one endothermic peak, related to the evaporation of the residue water, was observed for each sample. With increasing Fe content, this peak shifted gradually at high temperatures. When the temperature of 1000 °C was reached, a mass gain for all the samples was detected. It was seen that this increase in the mass percent was affected by Fe content. The SEM observations showed the all the as-prepared BCPs are composed of the rod-shaped particles, and the EDX confirmed the introduction of the co-dopants into the samples. It was concluded that some properties, especially the crystallinity and phase distribution, of the Mg-based BCPs can be easily controlled by Fe content.



	Ca (at.%)	P (at.%)	O (at.%)	Mg (at.%)	Fe (at.%)
0.35Mg-0.35Fe-BCP	21.40	14.67	63.29	0.36	0.28
0.35Mg-0.70Fe-BCP	21.82	13.67	63.58	0.30	0.63
0.35Mg-1.05Fe-BCP	20.84	14.19	63.53	0.32	1.12

Fig. 3 SEM micrographs and EDX analysis results of the as-prepared BCPs



**Fig. 4** DTA curves of the as-synthesized BCP samples

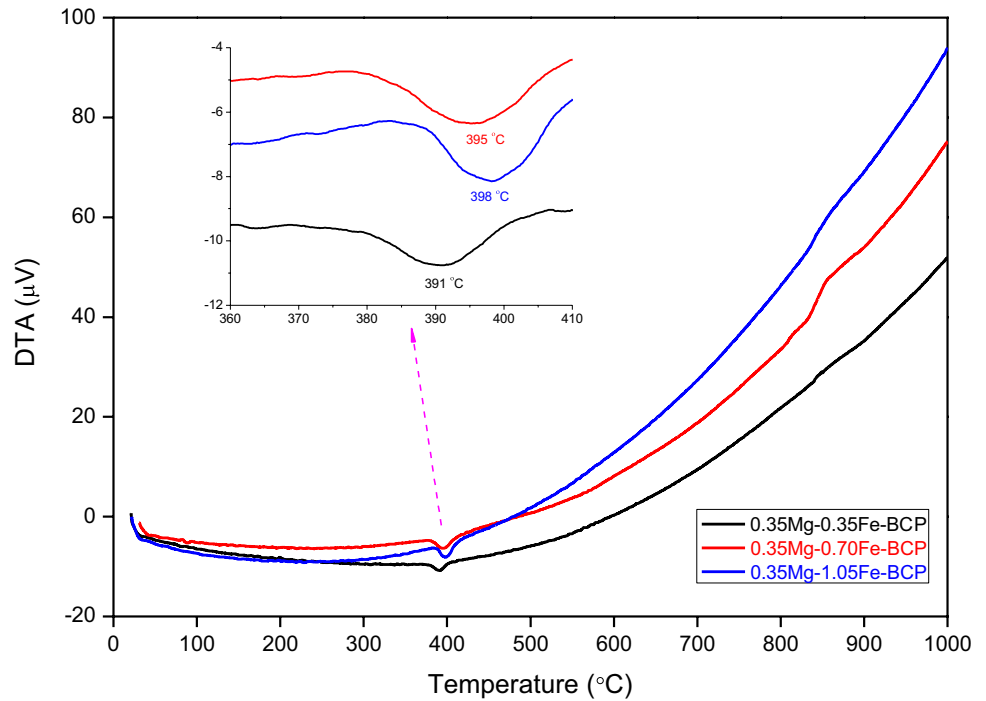
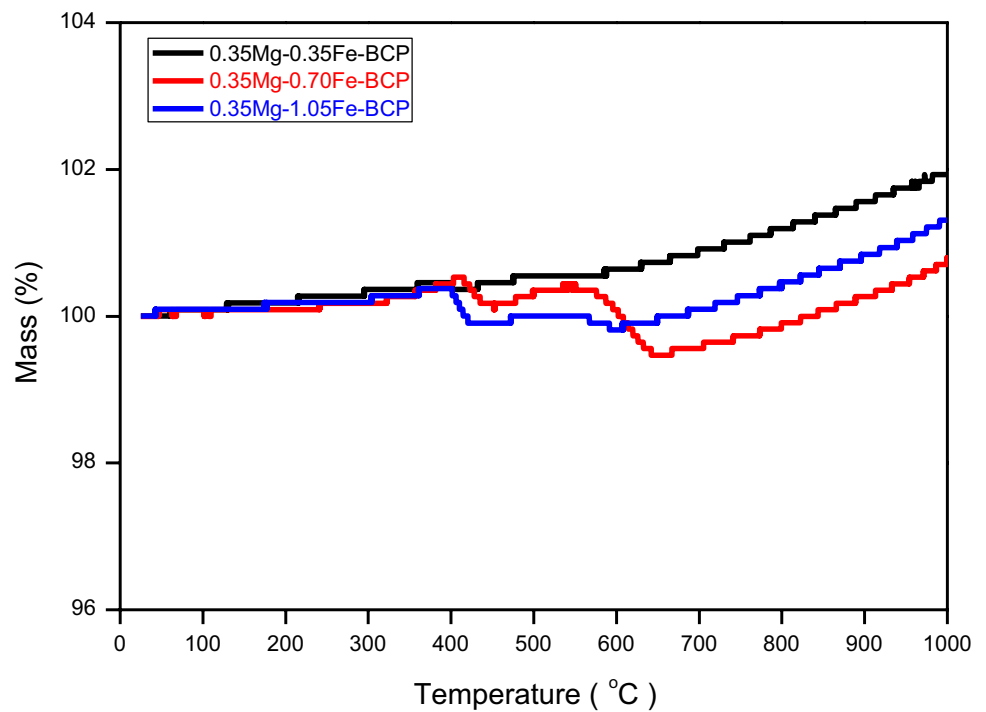


**Fig. 5** TGA curves of the as-produced BCPs



**Acknowledgements** This work was supported by the Management Unit of Scientific Research Projects of Firat University (FÜBAP) (Project Number: FF.18.16).

## References

1. S.V. Dorozhkin, Multiphasic calcium orthophosphate ( $\text{CaPO}_4$ ) bioceramics and their biomedical applications. *Ceram. Int.* **42**, 6529–6554 (2016)
2. S.V. Dorozhkin, Calcium orthophosphates. *Biomater* **1**, 121–164 (2011)

3. C.F. Marques, S. Olhero, J.C.C. Abrabtes, A. Marote, S. Ferreira, S.I. Vieira, J.M. Ferreira, Biocompatibility and antimicrobial activity of biphasic calcium phosphate powders doped with metal ions for regenerative medicine. *Ceram. Int.* **43**, 15719–15728 (2017)
4. Y.Z.K. Zhang, R. Zhao, X. Ye, X. Chen, Z. Xiao, X. Yang, X. Zhu, K. Zhang, Y. Fan, X. Zhang, Bone regeneration with micro/nano hybrid-structured biphasic calcium phosphate bioceramics at segmental bone defect and the induced immunoregulation of MSCs. *Biomaterials* **147**, 133–144 (2017)
5. J.M. Bouler, P. Pilet, O. Gauthier, E. Verron, Biphasic calcium phosphate ceramics for bone reconstruction: a review of biological response. *Acta Biomater.* **53**, 1–12 (2017)
6. S. Garai, A. Sinha, Three dimensional biphasic calcium phosphate nanocomposites for load bearing bioactive bone grafts. *Mater. Sci. Eng. C* **59**, 375–383 (2016)
7. N.F.A.C. Wahab, T.P. Kannan, Z. Mahmood, I. Ab. Rahman, H. Ismail, Genotoxicity assessment of biphasic calcium phosphate of modified porosity on human dental pulp cells using Ames and Comet assays. *Toxicol. In Vitro* **47**, 207–212 (2018)
8. T.W. Kim, H.S. Lee, D.H. Kim, H.H. Jin, K.H. Hwang, J.K. Lee, H.C. Park, S.Y. Yoon, In situ synthesis of magnesium-substituted biphasic calcium phosphate and in vitro biodegradation. *Mater. Res. Bull.* **47**, 2506–2512 (2012)
9. S. Gomes, A. Kaur, J.M. Greneche, J.M. Nedelec, G. Renaudin, Atomic scale modeling of iron-doped biphasic calcium phosphate bioceramics. *Acta Biomater.* **50**, 78–88 (2017)
10. O. Kaygili, J. Aust. *Ceram. Soc.* (2018). <https://doi.org/10.1007/s41779-018-0245-9>
11. Martin, J.D., 2004. Using X Powder: a software package for powder X-Ray diffraction analysis. D.L. GR 1001/04. ISBN: 84-609-1497-6, Spain. <http://www.xpowder.com>. Accessed 1 Apr 2019
12. O. Kaygili, Synthesis and characterization of Na<sub>2</sub>O–CaO–SiO<sub>2</sub> glass–ceramic. *J. Therm. Anal. Calorim.* **117**, 223–227 (2014)
13. O. Kaygili, S.V. Dorozhkin, T. Ates, A.A. Al-Ghamdi, F. Yakuphanoglu, Dielectric properties of Fe doped hydroxyapatite prepared by sol-gel method. *Ceram. Int.* **40**, 9395–9402 (2014)
14. B.D. Cullity, *Elements of X-ray diffraction*, 2nd edn. (Addison-Wesley Publishing Company, Boston, 1978)
15. O. Kaygili, S. Keser, Sol–gel synthesis and characterization of Sr/Mg, Mg/Zn and Sr/Zn co-doped hydroxyapatites. *Mater. Lett.* **141**, 161–164 (2015)
16. P. Kanchana, N. Lavanya, C. Sekar, Development of amperometric L-tyrosine sensor based Fe-doped hydroxyapatite nanoparticles. *Mater. Sci. Eng. C* **35**, 85–91 (2014)
17. W.Z. Yang, D.L. Zhou, G.F. Yin, G.D. Li, Surface modification of biphasic calcium phosphate bioceramic powders. *Appl. Surf. Sci.* **255**, 477–479 (2008)
18. A.K. Guha, S. Singh, R. Kumaresan, S. Nayar, A. Sinha, Mesenchymal cell response to nanosized biphasic calcium phosphate composites. *Colloids Surf. B* **73**, 146–151 (2009)
19. T.W. Kim, Y.M. Park, D.H. Kim, H.H. Jin, K.K. Shin, J.S. Jung, H.C. Park, S.Y. Yoon, In situ formation of biphasic calcium phosphates and their biological performance in vivo. *Ceram. Int.* **38**, 1965–1974 (2012)
20. S.T. AbdulQader, I. Ab Rahman, H. Ismail, T.P. Kannan, Z. Mahmood, A simple pathway in preparation of controlled porosity of biphasic calcium phosphate scaffold for dentin regeneration. *Ceram. Int.* **39**, 2375–2381 (2013)
21. Z. Mohammadi, A.S.M. Mesgar, F. Rasouli-Disfani, Preparation and characterization of single phase, biphasic and triphasic calcium phosphate whisker-like fibers by homogenous precipitation using urea. *Ceram. Int.* **42**, 6955–6961 (2016)
22. L. Zhang, C. Zhang, R. Zhang, D. Jiang, Q. Zhu, S. Wang, Extraction and characterization of HA/β-TCP biphasic calcium phosphate from marine fish. *Mater. Lett.* **236**, 680–682 (2019)
23. M. Tavakkoli-Gilavan, H. Abdizadeh, M.R. Golobostanfard, Biomineralization behavior of electrophoretic-deposited hydroxyapatite-tricalcium phosphate biphasic composite. *Appl. Surf. Sci.* **458**, 988–995 (2018)
24. B. Li, X. Chen, B. Guo, X. Wang, H. Fan, X. Zhang, Fabrication and cellular biocompatibility of porous carbonated biphasic calcium phosphate ceramics with a nanostructure. *Acta Biomater.* **5**, 134–143 (2009)
25. L. Nie, D. Chen, J. Suo, P. Zou, S. Feng, Q. Yang, S. Yang, S. Ye, Physicochemical characterization and biocompatibility in vitro of biphasic calcium phosphate/polyvinyl alcohol scaffolds prepared by freeze-drying method for bone tissue engineering applications. *Colloids Surf. B* **100**, 169–176 (2012)
26. A.H. Rajabi-Zamani, A. Behnamghader, A. Kazemzadeh, Synthesis of nanocrystalline carbonated hydroxyapatite powder via nonalkoxide sol–gel method. *Mater. Sci. Eng. C* **28**, 1326–1329 (2008)
27. S. Raynaud, E. Champion, D. Bernache-Assollant, P. Thomas, Calcium phosphate apatites with variable Ca/P atomic ratio I Synthesis, characterisation and thermal stability of powders. *Biomaterials* **23**, 1065–1072 (2002)

**Publisher's Note** Springer Nature remains neutral with regard to jurisdictional claims in published maps and institutional affiliations.